

## Crystallization kinetics of polylactide: Reactive plasticization and reprocessing effects



Berit Brüster<sup>a</sup>, Antonio Montesinos<sup>b</sup>, Pauline Reumaux<sup>a</sup>, Ricardo A. Pérez-Camargo<sup>b</sup>, Agurtzane Mugica<sup>b</sup>, Manuela Zubitur<sup>c</sup>, Alejandro J. Müller<sup>b,d,\*\*</sup>, Philippe Dubois<sup>a</sup>, Frédéric Addiego<sup>a,\*</sup>

<sup>a</sup> Luxembourg Institute of Science and Technology, Materials Research and Technology (MRT) Department, National Composite Center of Luxembourg (NCC-L), 5 Rue Bommel, ZAE Robert Steichen, L-4940 Hautcharage, Luxembourg

<sup>b</sup> POLYMAT and Polymer Science and Technology Department, Faculty of Chemistry, University of the Basque Country UPV/EHU, Paseo Manuel de Lardizabal 3, 20018 Donostia-San Sebastián, Spain

<sup>c</sup> Chemical and Environmental Engineering Department, Polytechnic School, University of the Basque Country UPV/EHU, 20018 Donostia-San Sebastián, Spain

<sup>d</sup> Ikerbasque, Basque Foundation for Science, Bilbao, Spain

### ARTICLE INFO

#### Keywords:

Poly(lactide)  
Reactive extrusion  
Plasticization  
Reprocessing  
Crystallization kinetics

### ABSTRACT

This work focused on the determination of crystallization kinetics of neat polylactide (PLA) and a plasticized grade of PLA obtained by reactive extrusion (pPLA), as a function of thermomechanical recycling. In particular, the materials were submitted to repeated extrusion and injection procedures to simulate recycling. Prior reprocessing, spherulitic growth rate determined by polarized light optical microscopy indicated that pPLA crystallized into much smaller spherulites as compared to PLA. This finding was explained by a lower nucleation energy barrier promoted by the plasticization of pPLA. Isothermal overall crystallization kinetics were determined by differential scanning calorimetry measurements. It was found that pPLA crystallized much faster than neat PLA due to the plasticization effect. With increasing the number of processing cycles up to 5, PLA crystallization rate gradually increased, while at the same time that of pPLA remained constant. This result was explained by more important degradation mechanisms in PLA as compared to pPLA that enhanced chain mobility, as shown by molecular weight measurements. Moreover, pPLA had a very high initial chain mobility that is maintained regardless of the number of processing cycles. However, the final crystallinity degree was lower in reprocessed pPLAs, as grafting and cross-linking reactions produced during reactive extrusion interrupt crystallizable linear crystallizable sequences and reduced the amount of crystals formed.

### 1. Introduction

Poly (lactic acid) (PLA) is currently being considered a sustainable alternative to conventional petroleum-based polymers, such as polyethylene terephthalate (PET), for packaging applications [1]. The environmental impact of PLA, which is bio-based and (bio) degradable, is lower than that of PET in term of life cycle assessment (LCA), facilitating a reduction of global warming, fossil energy consumption, and human toxicity [2,3].

However, neat PLA is brittle at room temperature, as opposed to PET, and typically amorphous, as its rate of crystallization is much slower than the cooling rates applied during commercial plastic processing operations. As its glass transition is only 55–60 °C, its

applications are limited to relatively low temperatures, unless crystallization can be induced.

To overcome brittleness, PLA can be blended with other polymers, such as poly ( $\epsilon$ -caprolactone), poly (butylene succinate) and poly (hydroxy butyrate), among others [4] or with plasticizers, which enhanced the mechanical properties of PLA including ductility and toughness [5]. Some of the plasticizers that have been blended with PLA are for example citrate esters [6], poly (ethylene glycol)s of various kinds, glucose monoesters and partial fatty acid esters [7]. Because of some drawbacks of the conventional plasticizers as leaching and potential toxicity, several epoxidized vegetal oils have been studied and reported as environmentally friendly plasticizers [8].

It is worth noting that plasticizer leaching towards PLA surface can

\* Corresponding author.

\*\* Corresponding author POLYMAT and Polymer Science and Technology Department, Faculty of Chemistry, University of the Basque Country UPV/EHU, Paseo Manuel de Lardizabal 3, 20018 Donostia-San Sebastián, Spain.

E-mail addresses: [alejandrojesus.muller@ehu.es](mailto:alejandrojesus.muller@ehu.es) (A.J. Müller), [frederic.addiego@list.lu](mailto:frederic.addiego@list.lu) (F. Addiego).

<https://doi.org/10.1016/j.polydegstab.2018.01.009>

Received 14 November 2017; Received in revised form 4 January 2018; Accepted 7 January 2018

Available online 09 January 2018

0141-3910/ © 2018 Elsevier Ltd. All rights reserved.

also be avoided by reactive extrusion, in which the plasticizer is grafted onto the PLA backbone. This process enables stability of the plasticizer within PLA matrix, even after long term storage [9,10]. Reactive extrusion has been recently performed in our previous work, by mixing PLA with poly (ethylene glycol) methyl ether acrylate (acryl-PEG) in the presence of a 2,5-dimethyl-2,5-di (tert-butylperoxy) hexane (L101) as a free-radical initiator leading to a dispersion of rubbery poly (acryl-PEG)-based inclusions grafted to the partially cross-linked PLA matrix [9,10].

The management of PLA waste has to be optimized to retain the environmental benefits related to its production stage. It has been shown that incineration, followed by chemical recycling and composting, are the less detrimental scenarios for the environment, while landfill without energy recovery procedure is the worst case [3]. As alternative end-of-life scenario for PLA, thermo-mechanical recycling by reprocessing and reuse, as a conventional thermoplastic, increases energy saving and reduces renewable resources consumption as compared to incineration [11]. However, biodegradation should not be triggered prior to thermo-mechanical recycling [12].

Thermo-mechanical recycling of bioplastics and in particular PLA, has been investigated for the past decade at laboratory scale, which makes this end-of-life scenario an emerging activity [13–17]. It has been shown that PLA undergoes a constant decrease of its molecular weight during multiple injection molding cycles, attaining a 64% decrease of its weight average molecular weight ( $M_w$ ) after 7 cycles [13]. This decrease of molecular weight during recycling was also supported by a viscosity decrease [13,15], and was explained by chain thermo-mechanical degradation.

Multiple reprocessing by extrusion or injection also cause a progressive decrease of mechanical properties, such as toughness, tensile strength, tensile stress at break, and tensile strain at break as a result of the decrease in molecular weight [13,14].

The mechanical performance of recycled PLA is non-suitable for its initial application specifications, unless stabilizers [13] or virgin PLA (e.g., 50%–80%) are added to retain mechanical properties [17]. The influence of thermo-mechanical recycling on the physico-chemical properties of plasticized PLA obtained by reactive extrusion have been investigated in our previous work [18]. In the specific case of the thermal properties, chain scission increased chain mobility decreasing the glass transition, crystallization and cold crystallization temperatures and increasing the percentage of crystallinity of the samples as the number of injection cycles was increased.

In order to evaluate the plasticized PLA and/or recycled PLA, it is of high importance to control crystallinity for increasing dimensional stability and improving mechanical properties. In fact, such relationships have been recently reviewed by Müller et al. [19] on PLA-based materials.

In the present work, reactive extrusion of PLA with acryl-PEG in the presence of a free-radical initiator has been performed in order to obtain a plasticized PLA (pPLA). Then, a recycling process has been simulated by the application of several extrusion and injection molding cycles for neat PLA and pPLA. The tensile behavior, the molecular weight (i.e., by size exclusion chromatography), thermal properties (i.e., by differential scanning calorimetry), structure (i.e., by X-ray diffraction) and morphology (i.e., by atomic force microscopy and polarized light optical microscopy) have been determined for neat and reprocessed materials. Moreover, the overall crystallization kinetics was determined by isothermal DSC experiments. The influence of the grafted plasticizer and recycling-induced degradation was simultaneously studied for the first time, as far as the authors are aware.

## 2. Experimental section

### 2.1. Materials

The PLA grade 4042D from NatureWorks, containing 4.2 mol.% D-

isomeric units, was employed. As in our previous work, reactive extrusion of PLA was conducted with acryl-PEG ( $M_n \approx 480 \text{ g mol}^{-1}$ ) as plasticizer, and Luperox 101 (L101) as free-radical initiator, both supplied by Sigma-Aldrich. Processing cycles of plasticized PLA were conducted as specified below [9,10].

### 2.2. Processing

#### 2.2.1. First processing cycle of pPLA

The first processing cycle of pPLA consisted of these successive steps: (i) PLA pellets drying, (ii) reactive extrusion of PLA pellets with acryl-PEG and L101 to produce continuous strands of plasticized PLA (pPLA), (iii) grinding of pPLA strands into flakes, (iv) drying of pPLA flakes, and (v) injection molding of pPLA flakes into tensile specimens.

Extrusion into continuous strands of diameter 3–5 mm was conducted with a twin-screw micro-compounder DSM XPlore 15 cc at a temperature of 180 °C using nitrogen as purge gas. When reactive extrusion was performed, PLA pellets were first introduced into the extruder, whereas Acryl-PEG and L101 were previously mixed in a glass vial and then introduced into the extruder with a syringe to react with molten PLA. The total extrusion duration was 5 min with recirculation, while the screw speed was adjusted to 50 rpm. The grinding steps were done with a Laboratory grinder Wanner Baby B08.10 with toothed rollers of 4 mm enabling to produce flakes with size  $\leq 4 \text{ mm}$ .

A Haake MiniJet II from ThermoScientific was employed to perform injection molding of the different materials. The melt temperature in the cylinder and mold temperature were 180 and 65 °C, respectively. The injection pressure was set to 700 bars for an injection time of 5 s, while after injection a post-pressure of 100 bars was applied during 3 s to compensate material shrinkage. The injection mold supplied by ThermoScientific enabled the production of ASTM D638 type V tensile specimens (overall length 63.5 mm, overall width 9.53 mm, width of the narrow section 3.18 mm, thickness 4 mm).

#### 2.2.2. Multiple number of processing cycles of pPLA

Further processing cycles of pPLA were conducted to simulate multiple reprocessing. The procedure consisted of: (i) grinding of injected pPLA tensile specimens into flakes, (ii) drying of pPLA flakes, (iii) simple extrusion of pPLA flakes into strands, (iv) grinding of pPLA strands into flakes, (v) drying of pPLA flakes, and (vi) injection molding of pPLA flakes into tensile specimens. During each drying procedure, PLA and pPLA materials are heated overnight at 50 and 30 °C, respectively, in a vacuum oven Heraeus from ThermoScientific. The lower drying temperature of pPLA as compared to PLA was due to an important softening of pPLA flakes that clumped together during drying at 50 °C, and hence, a lower drying temperature was selected. Indeed, pPLA had a lower glass transition temperature as compared to PLA, as it will be demonstrated by DSC testing in the Results and Discussion section.

For simple extrusion procedures during reprocessing, the materials were extruded at 180 °C during 5 min by using a screw speed of 50 rpm and a nitrogen gas purge.

PLA/acryl-PEG/L101 systems with a composition of 79/20/1 wt%, denoted pPLA and 100/0/0 denoted PLA were produced. Both PLA and pPLA were subjected to the processing cycles summarized in Table 1. The number of processing cycles was actually indicated by the number of final shaping processes (x) in the material references PLA IMx and pPLA IMx with x = 1, 3, and 5, and where IM corresponded to injection moulding (Table 1). Note that in a previous paper [20], the final shaping process was compression moulding, and hence, the materials were named PLA CMx and pPLA CMx. For clarification, the evolution of PLA based materials properties was investigated as a function of the number of processing cycles (from 1 to 5), reprocessing starting from the processing cycle number 2.

**Table 1**  
Description of the processing cycles applied to the samples.

Sample	Number of reactive extrusion cycles	Number of simple extrusion cycles	Number of injection cycles
PLA IM1	–	1	1
PLA IM3	–	3	3
PLA IM5	–	5	5
pPLA IM1	1	–	1
pPLA IM3	1	2	3
pPLA IM5	1	4	5

### 2.3. Tensile testing

The tensile behaviour of the injected specimens was measured at 20 °C and at 60 mm min<sup>-1</sup> by means of a universal testing machine Instron 5967 (Norwood, MA, USA). The evolution of the engineering axial stress  $\sigma_{eng}$  was recorded as a function of the axial engineering strain  $\epsilon_{eng}$ . Based on the initial stroke length of 25 mm, the corresponding initial strain rate was  $\dot{\epsilon} = 4 \times 10^{-2} \text{ s}^{-1}$ . The tensile modulus  $E$ , the yield stress  $\sigma_y$ , the strain at the yield point  $\epsilon_y$ , the ultimate stress  $\sigma_u$ , and the ultimate strain  $\epsilon_u$  were calculated and averaged based on three specimens for the different processing cycle numbers.

### 2.4. Atomic force microscope (AFM)

The microstructure of pPLA materials as a function of the number of processing cycles was investigated by AFM. To this end, the pPLA samples were melted on a glass surface at 180 °C. After air cooling, the very smooth melted sides of the samples were studied by AFM, while special attention was paid on the topography and stiffness of the samples. AFM PeakForce QNM measurement mode was performed using a Dimension ICON AFM (Bruker, Santa Clara) with a RTESPA probe (40 N.m<sup>-1</sup> spring constant, 10 nm tip radius) to map the topography of these samples (amplitude imaging).

### 2.5. Size exclusion chromatography (SEC)

SEC analysis was conducted using the Agilent Technologies series 1200 apparatus working with a differential refractive index detection and two linear columns (PLgel 5  $\mu\text{m}$  Mixed-D, 200 g.mol<sup>-1</sup> <  $M_w$  < 400 kg.mol<sup>-1</sup>) in addition to a protection column. PLA IM1, PLA IM3 and PLA IM5 samples were dissolved in chloroform at a concentration of 1.5 mg.mL<sup>-1</sup> and filtered with a nylon acrodisc syringe filter (pore size of 0.45  $\mu\text{m}$ ) and the number average ( $M_n$ ) and weight average molecular ( $M_w$ ) weights standardized to polystyrene, as well as the molar-mass dispersity index ( $\mathcal{D} = M_w/M_n$ ) were determined for all the samples. For each material, three samples were tested and the average with standard deviation was provided.

### 2.6. Soxhlet extraction

Soxhlet extraction was applied to remove the non-grafted part of the plasticizer from the plasticized PLA matrix [10,20]. Approximately 1.5 g of pPLA was introduced in an extraction cellulose thimble placed in a 100 mL Soxhlet extractor. The latter was installed between a 500 mL round bottom flask filled with 350 mL of methanol (Carl Roth, > 99% for synthesis) and a reflux condenser. The soluble fraction of acryl-PEG was extracted for 24 h under reflux at 125 °C, while the solid fraction of pPLA was dried overnight at 50 °C in a Heraeus vacuum oven from ThermoScientific. The amount of non-grafted part was calculated by Equation (1):

$$EF (\%) = \frac{m_{\text{sample}} - m_{\text{solid}}}{m_{\text{sample}}} \times 100\% \quad (1)$$

where  $m_{\text{sample}}$  was the initial sample mass, and  $m_{\text{solid}}$  was the mass of the

solid sample after the extraction. The extracted fraction (EF) was determined three times per material and an average value with standard deviation was calculated.

### 2.7. Nuclear magnetic resonance spectroscopy (<sup>1</sup>H NMR)

<sup>1</sup>H NMR spectra of pPLA samples dissolved in deuterated chloroform (CDCl<sub>3</sub>, containing 0.3% of tetramethylsilane (TMS)) in concentrations of about 50 mg.mL<sup>-1</sup> were recorded with a Bruker AMX-500 at a frequency of 500 MHz and in a magnetic field of 11.6 T [20].

### 2.8. Polarized light optical microscopy (PLOM)

The crystalline superstructural morphology of PLA and pPLA was observed with a polarized light optical microscope (PLOM) Olympus BX51, equipped with a programmable heating system Mettler Toledo FP80 that enables temperature control with an accuracy of  $\pm 0.4$  °C. The samples were positioned between two glass slides and subjected to the following thermal stages: (i) heating from 20 to 180 °C at 20 °C.min<sup>-1</sup>, (ii) holding at 180 °C for 3 min, (iii) cooling to the desired crystallization temperature ( $T_c$ ) at  $-20$  °C.min<sup>-1</sup>, and (iv) holding at the  $T_c$  for selected times (i.e., isothermal crystallization). The two first stages were conducted to erase the thermal history of the materials, while crystalline structure was observed during the isothermal holding at the different  $T_c$ . Additionally, spherulitic growth rate was followed during isothermal crystallization. In the isothermal crystallization step, a minimum of three spherulites were followed during their free growth before they impinged on one another. Then, the radius of each spherulite was measured and plotted as a function of time. From this plot, the slope represents the spherulitic growth rate ( $G$ ) at the selected  $T_c$ .

### 2.9. Differential scanning calorimetry (DSC)

Calorimetric studies were conducted in a PerkinElmer Pyris 1 Differential Scanning calorimeter, equipped with an Intracooler 2P. All the experiments were performed under ultrapure nitrogen flow (20 mL.min<sup>-1</sup>), and the instrument was calibrated with indium and tin standards. Samples with a mass comprised between 3 and 5 mg were used.

#### 2.9.1. Non-isothermal scans

PLA and pPLA were subjected to DSC heating and cooling scans at 10 °C.min<sup>-1</sup>. The samples were first heated to 180 °C and kept at this temperature for 3 min, in order to erase thermal history. Subsequently the samples were cooled to 0 °C at  $-10$  °C.min<sup>-1</sup> while the corresponding cooling scan was recorded. Finally, the samples were heated again to register the second heating scan.

#### 2.9.2. Isothermal crystallization

Prior to isothermal crystallization testing, the isothermal  $T_c$  range employed for each sample was previously determined according to the detailed procedure recommended by Lorenzo et al. [21]. This procedure was employed in order to ensure that no crystallization occurred during the cooling step. Once the starting  $T_c$  (or minimum  $T_c$ ) was determined, the samples were subjected to the following successive stages: (i) heating from 25 to 180 °C at 10 °C.min<sup>-1</sup>; (ii) isothermal holding at 180 °C during 3 min; (iii) cooling to the selected  $T_c$  (starting on the minimum  $T_c$ ) at  $-60$  °C.min<sup>-1</sup> (iv) isothermal holding at  $T_c$  until saturation (e.g., 90 min for PLA) and (iv) heating from the selected  $T_c$  to 180 °C at 10 °C.min<sup>-1</sup> in order to register the melting behaviour after the isothermal step. The two first steps were performed to erase the thermal history of the sample, and afterward the crystallization kinetics was assessed during the isothermal holding at  $T_c$ . Several  $T_c$  values were employed in order to obtain the complete crystallization kinetics of each material.

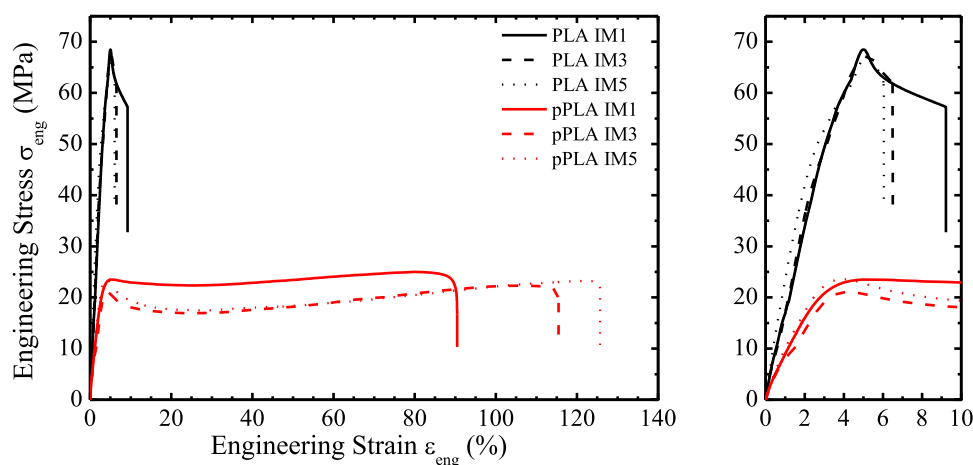


Fig. 1. Representative engineering stress-strain curves for PLA and pPLA after 1, 3, and 5 processing cycles with a zoom view of the behavior below 10% of strain.

### 3. Results and discussion

#### 3.1. Initial characterization of the reprocessed materials

##### 3.1.1. Mechanical characterization

During reprocessing, the material is subjected to mechanical shearing, high temperatures, and oxidation processes, among others, which typically can activate mechanical, chemical and thermal degradation or a combination of them. In a previous work, the recycling process of pPLA lead to a degradation of the PLA matrix, which was detrimental to the mechanical performance of the pPLA [20]. The reprocessing process in this work differs in the thermo-mechanical step from the previous work: injection molding was used instead of compression molding for the shaping step during reprocessing.

The representative tensile behavior for PLA and pPLA after one, three, and five processing cycles is presented in Fig. 1, while the corresponding mechanical parameters are listed in Table 2. Tensile properties of the material were expected to provide macroscopic insights of the influence of recycling. As already seen in previous studies, PLA is brittle at room temperature and the plasticization by reactive extrusion increases the ductility of the material [9,10,20]. For PLA, reprocessing leads to a slight decrease of the stress at yield from  $\sigma_y = 70.2$  MPa to  $\sigma_y = 66.7$  MPa after the first and fifth reprocessing, respectively. The elongation at break ( $\epsilon_u$ ) and the tensile modulus ( $E$ ) were nearly unaffected by the reprocessing, notwithstanding that PLA IM3 obtained the highest values.

For pPLA, the reprocessing had also just a slight impact on the mechanical performance. It is obvious that pPLA offered still a ductile behavior even after five processing cycles. Interestingly, the elongation at break increased from  $\epsilon_u = 91.1\%$  to  $\epsilon_u = 114.3\%$ , and to  $\epsilon_u = 127.0\%$  after the first, third and fifth processing cycle, respectively. This finding can be explained by microstructural transformations that are reported in the following section. It can be concluded that the reprocessing impacts neither PLA's nor pPLA's mechanical performance strongly.

Table 2

Mechanical parameters for PLA and pPLA after 1, 3, and 5 processing cycles with standard deviation.

	$E$ (MPa)	$\sigma_y$ (MPa)	$\epsilon_y$ (%)	$\sigma_u$ (MPa)	$\epsilon_u$ (%)
PLA IM1	2287 ( $\pm 301$ )	70.2 ( $\pm 1.5$ )	5.2 ( $\pm 0.3$ )	60.6 ( $\pm 3.1$ )	7.4 ( $\pm 1.0$ )
PLA IM3	2569 ( $\pm 294$ )	67.9 ( $\pm 1.6$ )	5.1 ( $\pm 0.1$ )	59.9 ( $\pm 3.4$ )	7.7 ( $\pm 1.7$ )
PLA IM5	2242 ( $\pm 332$ )	66.1 ( $\pm 0.7$ )	5.4 ( $\pm 0.5$ )	62.9 ( $\pm 2.0$ )	6.3 ( $\pm 0.4$ )
pPLA IM1	1178 ( $\pm 50$ )	23.2 ( $\pm 0.8$ )	5.3 ( $\pm 0.3$ )	26.1 ( $\pm 1.0$ )	91.1 ( $\pm 4.3$ )
pPLA IM3	1174 ( $\pm 64$ )	20.5 ( $\pm 1.8$ )	4.0 ( $\pm 0.4$ )	22.0 ( $\pm 0.2$ )	114.3 ( $\pm 1.1$ )
pPLA IM5	1272 ( $\pm 70$ )	23.3 ( $\pm 1.4$ )	3.9 ( $\pm 0.2$ )	22.9 ( $\pm 0.2$ )	127.0 ( $\pm 5.3$ )

##### 3.1.2. Microstructure investigation

Some typical images of pPLA as a function of processing cycle number recorded by AFM were represented in Fig. 2. The microstructure of pPLA consisted in a matrix with dispersed inclusions of rubbery poly (acryl-PEG). Prior reprocessing (Fig. 2a), it seems that the inclusions have a round to ellipsoidal shape, the ellipsoidal aspect being certainly due to the injection process. With reprocessing (Fig. 2b and c), the inclusion size decreases and the ellipsoidal aspect disappears so that inclusions have a heterogeneous shape.

An analysis of the images was conducted with the software ImageJ (Wayne Rasband, National Institutes of Health, USA). The used procedure consisted in transforming the color image into 8-bit grey level image, thresholding the grey level, and analyzing the resulting objects (inclusions). The final binary images are shown in Fig. 2. We found that the average area of the inclusions decreased from  $0.044 \mu\text{m}^2$  for pPLA IM1 (Figure 2d) to  $0.004 \mu\text{m}^2$  for pPLA IM5 (Fig. 2f). Note that for pPLA IM3, the average inclusion area was  $0.026 \mu\text{m}^2$  (Fig. 2e). Therefore, this decrease of inclusion size may be induced by the subsequent thermo-mechanical sollicitation of the material during the reprocessing, engendering a better dispersion state of the inclusions, without loss of rubbery poly (acryl-PEG). Considering that stress transfer between the PLA matrix and the rubbery inclusions is improved, facilitated by the grafting and cross-linking, a better dispersion of the inclusions may enhance such stress transfer explaining the increase of the ultimate strain of pPLA with reprocessing.

##### 3.1.3. Molecular structure characterization

The determination of the molecular weight is important to understand the influence of reprocessing cycles in the PLA samples. Due to the specific structure of pPLA with grafting and cross-linking of the plasticizer, the molecular weight analysis can just be done on the part of PLA without grafting and cross-linking.

Table 3 shows the Size Exclusion Chromatography (SEC) results for reprocessed PLA and pPLA. For PLA, as the number of processing cycles increases, the average molecular weights decrease, as expected. The molecular weight of PLA decreased after 5 processing cycles by 19%,

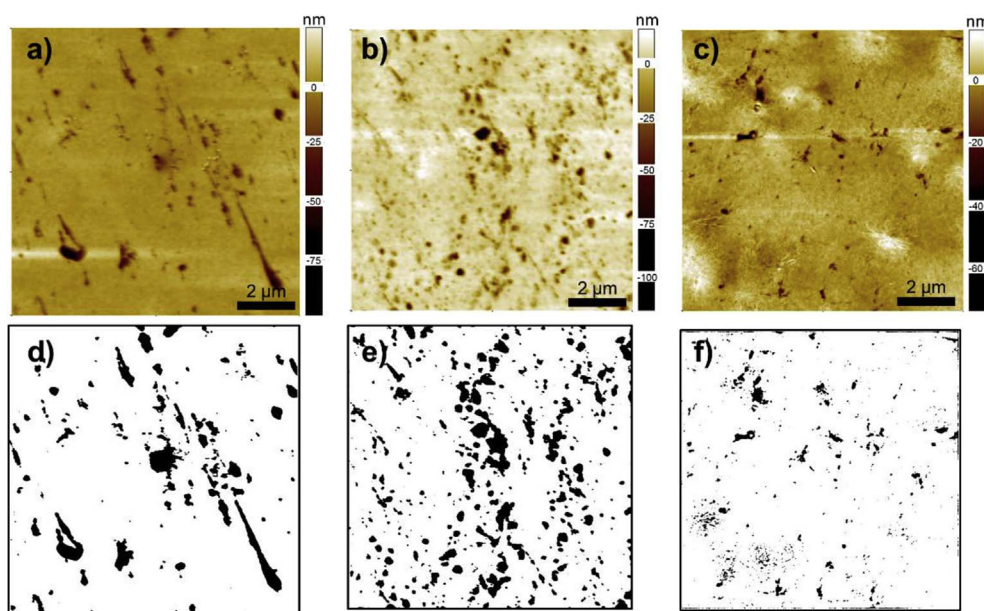


**Fig. 2.** AFM observations of pPLA as a function of processing cycle number in amplitude imaging mode a) to c), and after image treatment d) to f), in the case of PLA IM1 a) and d), pPLA IM3 b) and e), and pPLA IM5 c) and f).

**Table 3**  
Molecular weights from SEC measurements standardized to polystyrene.

Sample reference	$M_n$ ( $\text{kg}\cdot\text{mol}^{-1}$ )	$M_w$ ( $\text{kg}\cdot\text{mol}^{-1}$ )	$D$ $M_w/M_n$
PLA IM1	70	147	2.1
PLA IM3	70	147	2.0
PLA IM5	58	119	2.1
pPLA IM1	29	54	1.9
pPLA IM3	29	55	1.9
pPLA IM5	27	50	1.9

but the polydispersity of the material did not significantly change. This could be attributed to a chain scission degradation process through the formation of free radicals. Such kind of degradation has been described in the literature by Soroudi and Jakubowicz [17] and is in line with our previous work, in which no different functional groups from the original PLA were observed [20].

In the case of pPLA, the samples are not completely soluble for the SEC analysis. This fact is attributed to grafting and cross-linking between PLA and acryl-PEG, as in our previous work [20]. Both grafting and cross-linking occur during the reactive extrusion step, in which the L101 is able to provoke scissions in the PLA growing chains and at the same time cause a grafting process in between acryl-PEG and PLA chains. Nevertheless, it was possible to analyse the soluble part of PLA in pPLA by SEC. It is obvious that the molecular weight of pPLA's soluble part is much lower than in the neat PLA samples, which is attributed to the chain scission reactions induced by free radicals during the reactive extrusion. The molecular weight of this soluble PLA fraction decreased just slightly by 7.4%, while the polydispersity index was unaffected. Therefore, it can be concluded that pPLA matrix, at least the soluble part in chloroform, was less degraded than PLA matrix. It is important to mention that it was not possible to determine the soluble fraction of pPLA in chloroform because the non-soluble part of the material consisted in an unstable gel that made its analysis impossible. As a consequence, the quantitative characterization of the cross-linking in pPLA could not be done.

In order to prove the presence of grafting and cross-linking reactions during reactive extrusion of pPLA samples, the non-grafted plasticizer content has been determined by Soxhlet extraction [10,20]. Accordingly, the extracted fraction of plasticizer was about 6 wt% whatever the processing cycle was, corresponding to about one-third of the

overall plasticizer amount, which was 20 wt%.  $^1\text{H}$  NMR analysis of the pPLA materials revealed that its amount was constant to about 14 wt% during the reprocessing. As seen in a previous publication, the grafting and cross-linking hinder an exact determination of the plasticizer amount in pPLA, since the grafted and cross-linked part is just partially soluble [20]. The constant amounts of detected plasticizer fraction and extractable plasticizer fraction (see Table 4) indicate that the grafting and cross-linking points are not influenced by recycling. As a consequence, the decrease of inclusion size with reprocessing (Fig. 2), was not accompanied by a damage of grafting and cross-linking points, nor loss of rubbery poly (acryl-PEG).

#### 3.1.4. Non-isothermal DSC

Fig. 3 shows DSC first heating (Fig. 3a), cooling (after erasing thermal history) (Fig. 3b) and subsequent heating scans (Fig. 3c) for neat PLA, reprocessed PLA (IMx) and reprocessed plasticized PLA (pPLA IMx). The relevant thermal parameters, obtained from Fig. 3, are listed in Table 5.

Fig. 3a shows that neat PLAs (either with or without reprocessing) and pPLA (reprocessed) display several thermal transitions, such as the glass transition temperature ( $T_g$ ), cold crystallization ( $T_{cc}$ ) and melting ( $T_m$ ) temperatures during the first heating scan. The endothermic jump at temperatures around 60 °C is due to the glass transition.

In the case of PLA IM1, PLA IM2 and PLA IM3, an endothermic peak is shown just above  $T_g$  that is characteristic of enthalpic relaxation of the material, while this peak is not present for PLA pellets. This relaxation is due to a physical ageing of the PLA amorphous phase characterized by molecular rearrangements that drive the glassy material to a more ordered state closer to equilibrium. During physical ageing, the polymer loses enthalpy as free volume is decreased. During

**Table 4**  
Amount of plasticizer determined from  $^1\text{H}$  NMR measurements and amount of non-grafted plasticizer determined from Soxhlet extraction with methanol for pPLA samples after 1, 3, and 5 processing cycles.

Sample	PEG content (wt.%) from $^1\text{H}$ NMR	non-grafted amount of PEG (wt.%) from Soxhlet extraction
pPLA IM1	14.5	5.8 (± 0.1)
pPLA IM3	14.3	6.4 (± 0.6)
pPLA IM5	14.2	6.4 (± 0.1)

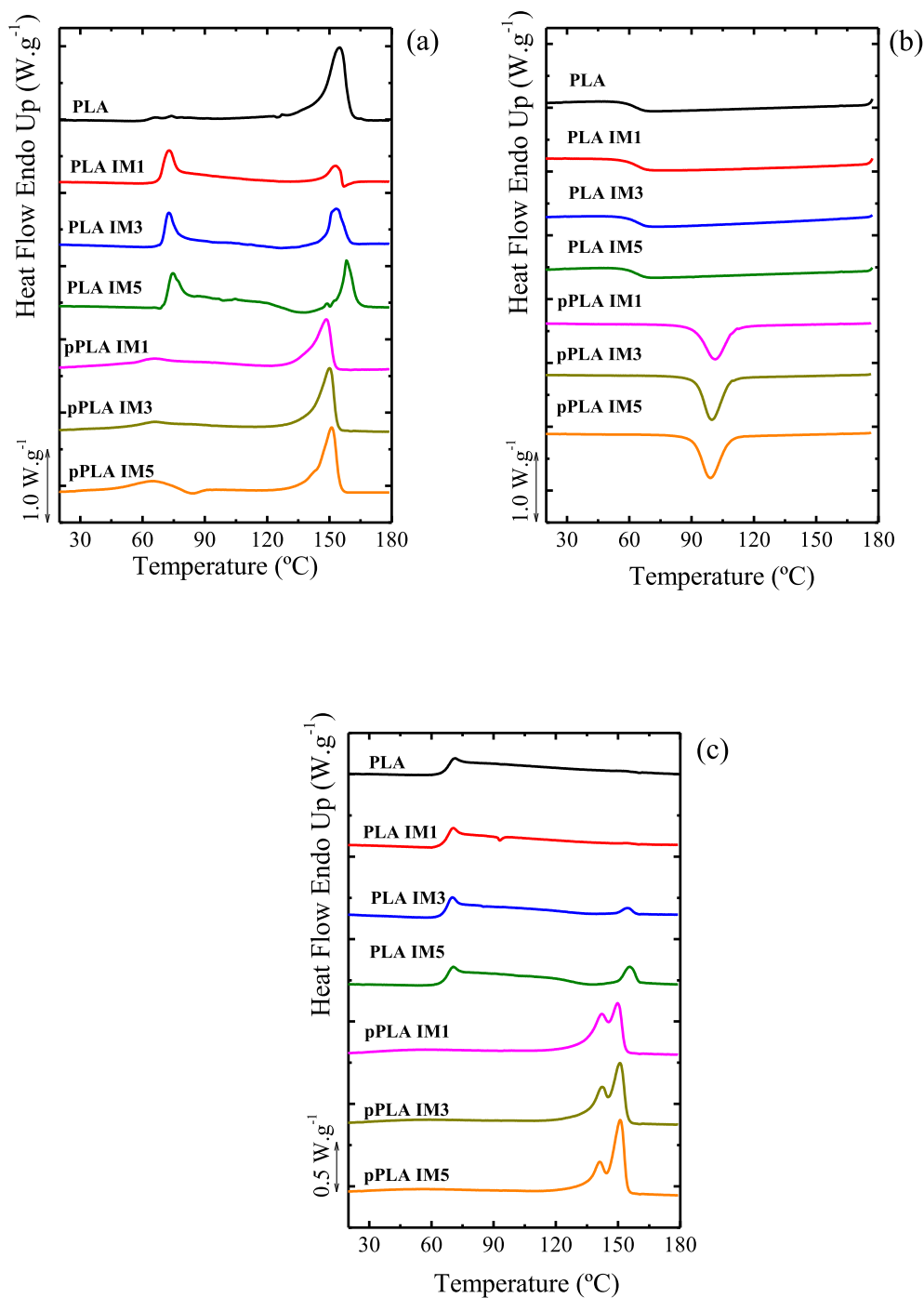


Fig. 3. DSC (a) first heating (b) cooling and (c) second heating scans for neat PLA, reprocessed PLA (PLA IM1, IM3 and IM5) and pPLA (pPLA IM1, IM3 and IM5).

Table 5

Thermal properties determined from DSC measurements. Glass transition ( $T_g$ ), cold crystallization ( $T_{cc}$ ) and melting ( $T_m$ ) temperatures; cold crystallization ( $\Delta H_{cc}$ ), melting ( $\Delta H_m$ ) and crystallization ( $\Delta H_c$ ) normalized enthalpies. Degree of crystallinity ( $X_c$ ).

Sample	First Heating						Cooling				Second Heating					
	$T_g$ (°C)	$T_{cc}$ (°C)	$\Delta H_{cc}^n$ (J.g <sup>-1</sup> )	$T_m$ (°C)	$\Delta H_m^n$ (J.g <sup>-1</sup> )	$X_c$ (%)	$T_g$ (°C)	$T_c$ (°C)	$\Delta H_c^n$ (J.g <sup>-1</sup> )	$T_g$ (°C)	$T_{cc}$ (°C)	$\Delta H_{cc}^n$ (J.g <sup>-1</sup> )	$T_m$ (°C)	$\Delta H_m^n$ (J.g <sup>-1</sup> )	$X_c$ (%)	
PLA	62.2	–	–	154.9	32	33.9	62.0	–	–	67.5	–	–	–	–	–	
PLA IM1	68.5	–	–	152.9	7	7.9	62.9	–	–	66.5	–	–	–	–	–	
PLA IM3	69.2	127.5	3	153.2	12	12.6	62.9	–	–	66.3	134.8	1	154.5	1	1.1	
PLA IM5	70.9	137.5	7	158.2	10	10.5	62.4	–	–	66.7	135.5	3	155.9	3	3.3	
pPLA IM1	60.2	–	–	148.6	21	22.1	–	101.5	21	–	–	–	141.9/149.9	24	26.1	
pPLA IM3	61.4	–	–	150.2	25	26.7	–	99.8	22	–	–	–	142.2/150.9	27	28.5	
pPLA IM5	58.5	85.2	4	151.2	26	28.0	–	99.1	23	–	–	–	140.9/150.9	23	24.4	

subsequent heating, the material recovers the enthalpy lost and an endothermic peak is observed [22].

The physical ageing process is accelerated by any factor that contributes to chain mobility. For instance, as annealing temperature below  $T_g$  is increased, the enthalpy relaxation is faster and more pronounced. Reductions in molecular weight or inclusion of plasticizers are factors that can also enhance enthalpy relaxation during physical ageing. In fact, recent studies on the physical ageing of PLA have demonstrated that nucleation is greatly enhanced by annealing below  $T_g$  [23,24]. The enthalpic relaxation process is related exclusively to the amorphous regions of the samples and will also be more noticeable in samples with a lower crystallinity degree [25,26].

One of the most important differences between PLAs and pPLAs shown in Fig. 3a is that both  $T_g$  and  $T_m$  are shifted to lower values in the case of all pPLAs as compared to PLAs. This behaviour is attributed to the effect of the plasticizer agent grafted on the pPLA (i.e., acryl-PEG).

When the samples are cooled from the melt at  $10^\circ\text{C}\cdot\text{min}^{-1}$  (see Fig. 3b) (i.e., after thermal history is erased), PLA samples with and without reprocessing cycles are not able to crystallize and only exhibit vitrification at  $T_g$  (see Fig. 3b), which is a general behaviour of commercial PLAs. As explained in the experimental part, the PLA employed here contains 4.2 mol.% of *D*-units, which interrupt the *L*-units and slow down the crystallization ability of the *L*-chains. When the cooling rate (in this case  $10^\circ\text{C}\cdot\text{min}^{-1}$ ) employed is faster than the crystallization rate of the material, the PLA chains are not able to crystallize.

In contrast, pPLAs are able to crystallize during cooling from the melt at  $10^\circ\text{C}\cdot\text{min}^{-1}$  (Fig. 3b). This enhanced non-isothermal crystallization ability is caused by the grafted and highly flexible acryl-PEG chains that can act as an internal or molecular plasticizer (decreasing  $T_g$  values and increasing chain mobility) that enhances PLA chain diffusion in between cross-linking points. Cross-linking points are defects along the chains that interrupt the linear crystallizable *L*-sequences along PLA chains, but it is clear that the cross-linking density must be very low. As the cross-linking density increases,  $T_g$  must also increase and eventually the plasticizing effect would be lost and chain rigidity as well as  $T_g$  increases would be observed.

Interestingly pPLAs do not show  $T_g$  neither during cooling or second heating scans (see Fig. 3b and c), as noted in previous works [10,20]. The origin of this phenomenon is unclear but some clarifications can be provided based on DMA results provided in Figure S1 of the Supplementary data, where the glass transition  $T_g$  of pPLA was clearly visible. In particular it was equal to  $56^\circ\text{C}$  for pPLA IM1 and  $66^\circ\text{C}$  for PLA IM1 demonstrating that reactive plasticization decreased  $T_g$  of  $10^\circ\text{C}$  as shown by DSC first heating results (Table 5). In the loss factor  $\tan \delta$  – temperature curves of pPLA the glass transition was characterized by a broader and lower peak as compared to PLA. If the relaxation peak width is related to a certain distribution of molecular movements or characteristic times of movement, and the relaxation peak height is related to the number of movements, it can be concluded that the molecular network of pPLA is much more complex than that of PLA. This complexity can be explained by the grafting and cross-linking reactions occurring during the reactive extrusion. The glass transition detection of this complex molecular network may be in general hard to observe by DSC due to the broad molecular movements required for the glass transition relaxation.

Fig. 3c shows the DSC second heating scans for all the materials. Both PLA and PLA IM1 do not show cold crystallization or melting peaks, a reflection of their slow non-isothermal crystallization kinetics. However, as the number of processing cycles increases, a cold crystallization peak appears that is followed by melting. Their associated enthalpies increased with the number of processing cycles, indicating an enhanced ability to crystallize as degradation increases with the number of cycles (see molecular weight decrease in Table 3). In the case of unmodified PLA chains, degradation proceeds by random chain scission. It is well documented [19] that the overall crystallization rate increases as the  $M_w$  values decrease from  $200\text{ kg mol}^{-1}$  down to

$10\text{ kg mol}^{-1}$ , encompassing the range of values reported in Table 3. This effect is mainly attributed to the enhanced molecular mobility and diffusion of PLA chains as their length is reduced.

Fig. 3c shows that all plasticized samples exhibit melting peaks corresponding to the crystals formed during the previous cooling runs (Fig. 3b), as no cold crystallization occurs during heating. The melting peaks of pPLA samples are lower than those of PLA samples. Two factors can explain in this case the lowering of the melting point: (a) the interruption of crystallizable linear sequences along the chains by grafting or cross-linking points and (b) the plasticization effect of the grafted acryl-PEG chains.

Another interesting result shown in Fig. 3c is that the melting points of pPLAs do not significantly vary with the number of processing cycles. The melting point of PLA is proportional to the molecular weight. It increases as a potential function, where for values of  $M_w$  lower than  $20\text{ kg mol}^{-1}$  the change with molecular weight is very large, but as the  $M_w$  increases, the increase in  $T_m$  values saturates and above  $80\text{ kg mol}^{-1}$ , it hardly changes at all when identical crystallization conditions are employed (see for instance, Fig. 3.3a in Ref. [19]). Therefore, even if pPLAs might experience some degree of degradation (as partially indicated by the SEC measurements), it is not large enough to be detected by changes in  $T_m$  values.

Another feature of the melting peaks on pPLA samples is that they are double melting peaks, whose origin is unclear. They can be attributed to the melting/recrystallization of metastable crystals, or to the melting of a double population of crystals having different lamellar thickness, or to the melting of both the  $\alpha'$  and  $\alpha$  crystalline phases [27]. It can be basically concluded that crystallization process in pPLA may engender crystals with different degrees of stability, certainly due to the presence of grafting and cross-linking points, and/or to a very fast crystallization kinetics. Reprocessing of pPLA did not significantly influence this double melting process.

Table 5 reports the crystallinity degree, which was calculated by Equation (2):

$$\%X_c = \frac{\Delta H_m - \Delta H_{cc}}{x_{PLA} \times \Delta H_{m,0}} \times 100\% \quad (2)$$

where  $x_{PLA}$  is the total weight amount of PLA (79 wt%), and  $\Delta H_{m,0}$  is the melting enthalpy of a 100% crystalline PLLA reported in the literature,  $\Delta H_{m,0} = 93.1\text{ J}\cdot\text{g}^{-1}$  [28].

Table 5 shows higher values of  $X_c$  for pPLA samples in comparison to PLA samples. This behavior is attributed to the enhanced plasticization effect (i.e., provided by grafting acryl-PEG to PLA chains), which increases the non-isothermal crystallization kinetics. As previously discussed, PLA samples can hardly crystallize under the applied scanning rates. This result reflects once more the large differences in crystallization kinetics of plasticized versus unmodified PLA under non-isothermal conditions at the employed scanning rates. In the case of isothermal crystallization, the crystallization conditions are very different, as the material is taken to a  $T_c$  value and left to crystallize until saturation, even if it takes a long time to achieve the completion of both primary and secondary crystallization.

### 3.2. Isothermal crystallization

#### 3.2.1. Morphology and spherulitic growth rate determined by polarized light optical microscopy (PLOM)

The spherulitic growth rate of PLA samples was measured by PLOM. Additionally, the morphological differences between PLA and pPLA were determined. Fig. 4 shows micrographs of (a) PLA-IM1 and (b) pPLA-IM1, taken after isothermal crystallization from the melt at 120 and  $128^\circ\text{C}$ , respectively. PLOM reveals for both samples, spherulitic superstructures with negative sign, as expected for PLA.

The nucleation density in pPLA materials was found to be much larger than for any PLA. In the example provided in Fig. 4 for pPLA-IM1, a particularly high  $T_c$  value (i.e.,  $8^\circ\text{C}$  higher than for PLA-IM1)

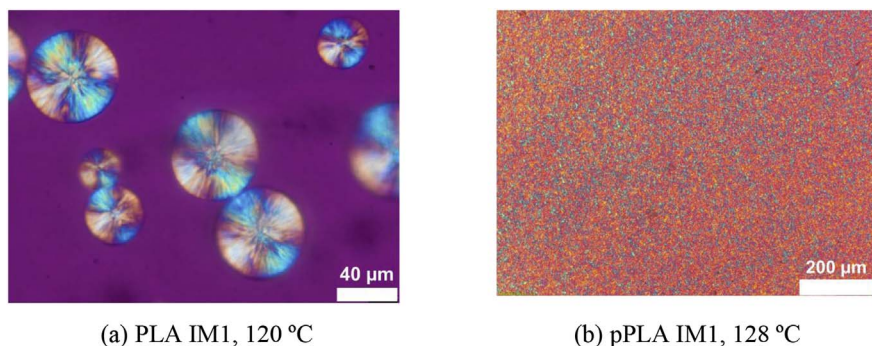


Fig. 4. (a) PLOM image of PLA IM1 spherulites after 37 min of isothermal crystallization at 120 °C, (b) PLOM image of pPLA IM1 spherulites after isothermal crystallization at 128 °C.

was employed in order to try to minimize the number of nuclei. The samples of pPLAs were found to nucleate instantaneously and with such a large number density of nuclei only very small spherulites can formed, as evidenced in the micrograph presented in Fig. 4b. The difference in nucleation density and nucleation rate can only be due to a lower nucleation energy barrier promoted by the plasticization effect of acrylic-PEG chains.

The experimental evidence presented here shows that pPLA develops a much higher nucleation density than PLA. This is consistent with literature findings indicating that long chain branched PLAs also exhibit a higher number of nucleation sites in comparison with linear PLAs. The reason behind this enhanced nucleation of long chain branched PLA is not known. Some authors have considered that this enhanced nucleation is due to the presence of branches and that branching points can be considered as nucleating points [29]. However, the notion that a branch point within a polymer chain can constitute a nucleus contradicts the large body of evidence indicating that chain branches are excluded from the crystal lattice in many polymeric materials. Any branch point or crosslinking point interrupts the linear crystallizable sequences in the polymer chain and therefore is excluded to the intervening amorphous layers [30]. Therefore, even though grafting and cross-linking may contribute to enhance nucleation, the fact that pPLA contains a plasticizer that enhances chain mobility is probably the dominant factor that reduces the energy barrier for primary nucleation in pPLA as compared to neat PLA.

Since the pPLAs exhibit such a high nucleation density (Fig. 4b), the spherulitic growth rate during isothermal crystallization was only determined on PLA samples with different number of processing cycles (i.e., IM1, IM3 and IM5). The spherulitic growth rate ( $G$ ) as a function of the isothermal crystallization temperature ( $T_c$ ) is plotted in Fig. 5.

Fig. 5 shows that as the number of processing cycles increases, the spherulitic growth rate also increases. The reason behind this acceleration in spherulitic growth is the decrease in molecular weight (i.e.,

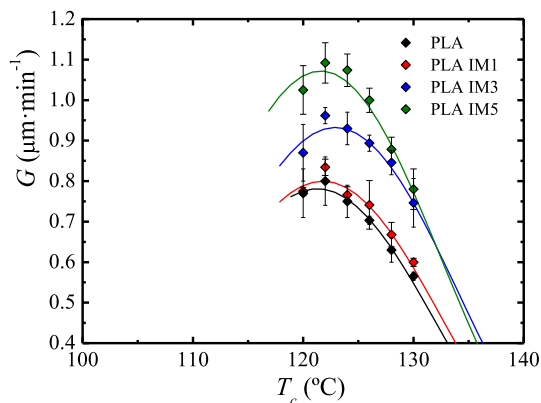


Fig. 5. Spherulitic growth rate ( $G$ ) as a function of isothermal crystallization temperature ( $T_c$ ) for PLA and reprocessed PLA (i.e., IM1, IM3 and IM5). Solid lines were added to guide the eye and correspond to the Lauritzen and Hoffman fits.

degradation induced by reprocessing, see Table 3). It is well-known [19] that the spherulitic growth rate of PLAs increase as the molecular weight decreases in the range 200 to 10 kg mol<sup>-1</sup>.

The data shown in Fig. 5 was fitted to the Lauritzen and Hoffman (LH) theory, according to the following expression [30,31]:

$$G(T) = G_0 \exp\left(\frac{-U^*}{R(T_c - T_\alpha)}\right) \exp\left(\frac{-K_g^G}{T_c \Delta T f}\right) \quad (3)$$

where  $G_0$  is a pre-exponential factor. The term on the left of Equation (3) is controlled by (i) diffusion, while the term on the right of the equation is controlled by (ii) nucleation. For (i) the parameters involved are the activation energy for the transport of the chains to the growing nuclei ( $U^*$ ) (a value of 1500 cal.mol<sup>-1</sup> is generally used); the gas constant ( $R$ ); the isothermal crystallization temperature ( $T_c$ ) and the temperature at which chain mobility ceases ( $T_\alpha$ ), which is usually calculated as  $T_\alpha = T_g - 30$  or  $T_g - 15$  (K), where  $T_g$  is the glass transition temperature. In the nucleation term (ii) of the equation, the parameters involved are: the secondary nucleation constant that is proportional to the energy barrier for spherulitic growth ( $K_g^G$ ) (defined by Equation (4)); the supercooling ( $\Delta T$ ) defined as the difference between equilibrium melting point ( $T_m^0$ ) and isothermal crystallization temperature ( $T_c$ ); and a temperature correction term defined as  $f = \frac{2T_c}{T_c + T_m^0}$ .

$$K_g^G = \frac{j b_0 \sigma \sigma_e T_m^0}{k \Delta h_f} \quad (4)$$

The terms in equation (4) are defined as:  $j$  is a constant number (2 or 4) taken as 2 for *Regime II*,  $b_0$  is the diameter of the chain,  $\sigma$  and  $\sigma_e$  correspond to the lateral and fold surface free energy, respectively,  $k$  is the Boltzmann constant and  $\Delta h_f$  is the heat of fusion of a perfect crystal. Since the product  $\sigma \sigma_e$  is obtained from Equation (4), the calculations of  $\sigma$  (by using the Hoffman modification of the Thomas-Stavely relation) [32],  $\sigma_e$  and  $q$ , which is the work done by the chain to form a fold, can be made according to Equations (5) and (6):

$$\sigma = 0.1 \Delta h_f \sqrt{a_0 b_0} \quad (5)$$

where  $a_0 b_0$  is the cross-sectional area of the chain.

$$q = 2 a_0 b_0 \sigma_e \quad (6)$$

The parameters obtained from the fittings are listed in Table 6.

Table 6  
Parameters obtained from fitting the LH theory\* to the data of Fig. 5.

Sample	$K_g^G \times 10^{-5}$ (K <sup>2</sup> )	$\sigma$ (erg.cm <sup>-2</sup> )	$\sigma_e$ (erg.cm <sup>-2</sup> )	$q \times 10^{13}$ (erg)	$R^2$
PLA	2.28	6.10	136	6.49	0.9992
PLA-IM1	2.21		135	6.29	0.9983
PLA-IM3	2.06		126	5.84	0.9984
PLA-IM5	2.24		133	6.36	0.9986

\*The LH fit was applied with the following parameters:  $a_0 = 4.5$  and  $b_0 = 5.17 \text{ \AA}$  [33];  $\Delta H_m^0 = 93.1 \text{ J.g}^{-1}$  [28];  $T_\alpha = T_g - 15 = 48 \text{ °C}$ ,  $T_m^0 = 180 \text{ °C}$ .

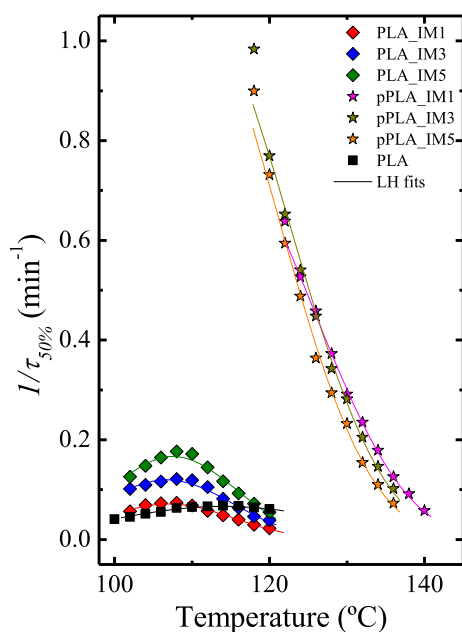


Fig. 6. Overall crystallization rate ( $1/\tau_{50\%}$ ) as a function of isothermal crystallization temperature for neat PLA, reprocessed PLA and pPLA (IM1, IM2 and IM3). The solid lines represents fits to the Lauritzen and Hoffman (LH) theory.

The lines that pass through the data points in Fig. 5 are the corresponding fittings of the LH theory. Even though the fittings seem adequate (see correlation coefficients in Table 6), the scattering of the data and the relatively narrow temperature range examined lead to very similar values of the LH parameters ( $K_g^G$ ,  $\sigma_e$  and  $q$ ) for neat and reprocessed PLAs. Even though the LH results are similar for all the samples, it is important to note that the values obtained are lower in magnitude as compared to the fitting parameters obtained by using the same theory on the overall crystallization rate data obtained by DSC, a fact that will be discussed below.

### 3.2.2. Overall isothermal crystallization kinetics by DSC

Isothermal DSC experiments were employed to determine the overall crystallization kinetics, which includes both primary nucleation and crystal growth. The inverse of the half-crystallization time is employed as a value proportional to the overall crystallization rate. Note that spherulitic growth rates only take into account crystal growth.

DSC experiments allow the determination of the isothermal overall crystallization kinetics for almost all of the samples employed in this work. The overall crystallization rate ( $1/\tau_{50\%}$ ) as a function of the isothermal crystallization temperature is shown in Fig. 6.

The presence of grafting and cross-linking points interrupts the crystallizable linear sequences of the PLA chains. Therefore, the presence of the plasticizer and the changes in the structure of the PLA chains are bound to affect the crystallization kinetics and recyclability of PLA.

A remarkable difference on the crystallization kinetics of PLA and pPLA was noted. In particular, pPLA crystallized much faster and requires less supercooling than PLA. At a temperature of 120  $^{\circ}\text{C}$ , the difference is almost one order of magnitude. Such difference can be attributed to the enhanced plasticization effect explained above.

Another important result is that the samples also differ in their responses to the number of processing cycles. In the case of reprocessed PLA, as the number of processing cycles increases, the overall crystallization rate also increases. This behaviour is expected on the basis of the increasing degradation of the samples with the increase in processing cycles (see Table 3). In this case, both nucleation and growth contributions are taken into account, and the results are consistent with those presented in Fig. 5 for spherulitic growth only.

In contrast, for the pPLA samples the overall crystallization rates remain almost constant regardless of the number of reprocessing cycles applied. As in the case of the non-isothermal DSC results that revealed constant  $T_m$  values for all pPLA samples, it would seem that if degradation is occurring during reprocessing, it is not so significant to affect the crystallization rate of pPLA samples. This is probably related to the cross-linked structure of the pPLA chains which could be significantly more degradation resistant than linear and non-modified PLA chains.

The enhanced plasticization effect as well as the influence of the reprocessing process on PLA and pPLA was also demonstrated by following the crystallization kinetics from the glassy state with XRD experiments. Such results are presented in Figure S2 of the Supplementary data.

An indirect evidence of partial grafting and cross-linking in pPLA can be obtained by calculating the final crystallinity achieved by the samples (i.e., until saturation) during isothermal crystallization. The  $X_c$  calculation was performed according to Equation (2) (i.e., the value of  $\Delta H_c$  was obtained directly for each isotherm by the Origin<sup>®</sup> plug-in developed by Lorenzo et al. [21]), but in this case  $\Delta H_m$  corresponds to the isothermal crystallization enthalpy, whereas  $\Delta H_{cc} = 0$ . A comparison of the  $X_c$  values for PLA and pPLA samples as a function of isothermal crystallization temperature is represented in Fig. 7.

In Fig. 7, it is observed that above the dashed line, whatever the imposed crystallization temperature, reprocessed PLA samples attained a crystallinity degree comprised between 25% and 45%, whereas below the dashed line, reprocessed pPLA samples attained  $X_c$  values between 20% and 25%. The much lower saturation crystallinity for the pPLA samples clearly indicates that the presence of cross-links and grafting points interrupts the crystallizable linear PLA chains and limit the amount of material that can crystallize. Therefore, the strategy of grafting the plasticizer chains can induce faster crystallization in isothermal conditions but the achieved final degree of crystallinity will be limited by the topology of the resulting chains. The defects along the pPLA chains (cross-linking points and grafting points) are excluded from the crystallization front to the amorphous regions increasing their

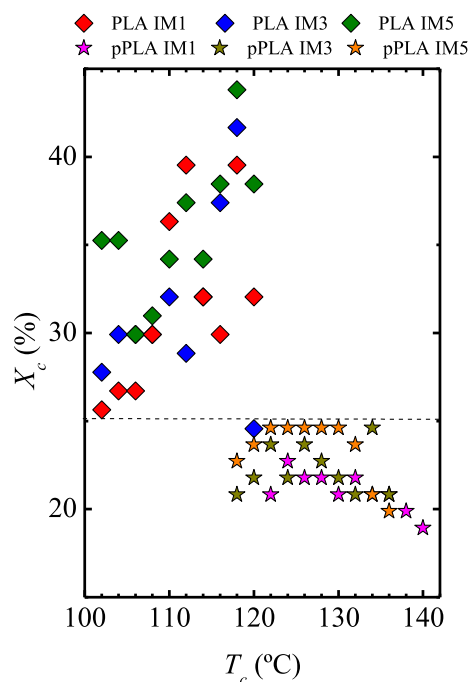


Fig. 7. Evolution of the final crystallinity  $X_c$  of the materials as a function of the crystallization temperature  $T_c$ . The  $X_c$  values were calculated from the crystallization isotherms of each material obtained during isothermal DSC experiments. The dashed line is to guide the eye.

density with time.

It is worth noting that the  $X_c$  values obtained for pPLA are similar to those measured during non-isothermal testing. In contrast, for the neat and reprocessed PLA, the  $X_c$  values are much larger for isothermal tests, because the materials are allowed to crystallize until saturation, as crystallization time is much longer (usually 30 min–40 min). Note that during a non-isothermal cooling scan, the materials can only crystallize during the short time span given by the cooling rate applied.

The overall isothermal crystallization kinetics can be modelled by the well-known Avrami equation [34–36].

$$1 - V_c(t - t_0) = \exp(-k(t - t_0)^n) \quad (7)$$

where  $V_c$  is the relative transformed volume fraction at time  $t$ ,  $n$  is the Avrami index,  $t_0$  is the induction time (i.e., the time elapsed at  $T_c$  before crystallization starts), and  $k$  is the Avrami rate constant, which is proportional to both nucleation and growth rates [21]. The fits to the Avrami equation (see Equation (7)) were performed using the Origin® plug-in developed by Lorenzo et al. [21]. Examples of the excellent fits obtained can be seen in Figure S4 of the Supplementary data.

The parameter  $n$ , is basically a complex kinetic order parameter that reflects how the overall kinetics depends on crystal dimensionality and nucleation mechanism. The Avrami index values obtained for all samples varied between 2.5 and 3.5 (see Table S3). Such values can be approximated to 3 and 4, which correspond to instantaneously nucleated spherulites or sporadically nucleated spherulites, respectively. No trends can be detected in the variation of the Avrami index with the number of processing cycles or crystallization temperatures. With regards to  $k$  values, once they are normalized by elevating them to the  $1/n$  power (so that similar time units are obtained in all cases irrespective of  $n$  value), they show very similar trends as those reported in Fig. 6, as can be seen in Figure S5 in the Supplementary data.

If  $G$  (T) in Equation (3) is substituted by  $1/\tau_{50\%}$  (T), then the Lauritzen and Hoffman model can be used to fit DSC data concerning the evolution of half-crystallization time with the imposed crystallization temperature [37]. In this case,  $K_g^\tau$  is considered as a constant that is proportional to the energy barrier for both nucleation and growth. The correlation between experimental data and the LH fits are shown in Fig. 6, while the obtained fitting parameters are reported in Table 7. For the recorded data range, a good correlation coefficient was obtained.

The most important trend that can be observed in Table 7 is that  $K_g^\tau$  values are at least twice as high for PLA and reprocessed PLA than those values obtained for pPLA samples. Similar trends are exhibited by  $\sigma_e$  and  $q$  values. These values are reasonable, since plasticized pPLA samples have much higher overall crystallization rates than all PLA samples. Another expected result is that  $K_g^\tau$  values are also much higher in the case of PLA samples (about 2.5 times) than  $K_g^G$  values (see Table 6), as the first values contained contributions from both nucleation and growth, while the latter ones depend only on spherulitic

**Table 7**

Parameters of LH model; parameter proportional to the energy barrier for nucleation and growth ( $K_g^\tau$ ), fold surface free energy ( $\sigma_e$ ), lateral surface free energy ( $\sigma$ ), work required for folding ( $q$ )\* and correlation coefficient for the LH plots ( $R^2$ ).

Sample	$K_g^\tau \times 10^{-5}$ (K <sup>2</sup> )	$\sigma$ (erg.cm <sup>-2</sup> )	$\sigma_e$ (erg.cm <sup>-2</sup> )	$q \times 10^{12}$ (erg)	$R^2$
PLA	5.83	6.10	337	1.55	0.9994
PLA IM1	4.80	6.10	297	1.38	0.9994
PLA IM3	5.74		351	1.63	0.9988
PLA IM5	4.94		305	1.42	0.9991
pPLA IM1	2.09	6.10	127	0.59	0.9994
pPLA IM3	2.42		148	0.69	0.9978
pPLA IM5	2.61		160	0.74	0.9984

\*The LH calculations were performed with the following parameters:  $a_0 = 4.5 \text{ \AA}$ ;  $b_0 = 5.17 \text{ \AA}$  [33];  $\Delta H_m^0 = 93.1 \text{ J.g}^{-1}$  [28];  $T_\alpha = T_g + 30 = 30 \text{ }^\circ\text{C}$ ;  $U^* = 1500 \text{ cal.mol}^{-1}$ ;  $T_m^0 = 180 \text{ }^\circ\text{C}$  [38].

growth (see Ref. [37]). On the other hand, the fitting parameters reported in Tables 6 and 7 do not show a significant variation with the number of processing cycles. A result that is expected in the case of the pPLA samples, because their crystallization kinetics seem to be independent of reprocessing (at least in the limited number of processing cycles explored in this work). In the case of PLA samples, it is possible that the small changes observed in crystallization kinetics are not important enough to have an influence on the fitting parameters of the LH model.

#### 4. Conclusions

Acryl-PEG was successfully grafted and even cross-linked on the PLA matrix through reactive extrusion, obtaining pPLA. Despite the fact that the grafting and cross-linking represent interruptions on the crystallization of the PLA, the grafted acryl-PEG acts as an enhanced plasticizer (i.e., because is grafted to the PLA backbone) that in fact improved remarkably the nucleation and the crystallization rate of PLA under non-isothermal and isothermal conditions. Although, at the same time the grafted and cross-linked acryl-PEG chains limited the percentage of crystallinity that can be obtained under isothermal conditions in comparison with neat PLA.

Recycling procedures were simulated through repeated processing cycles of extrusion and injection. The tensile behavior of PLA and pPLA was measured to get macroscopic information about the effect of recycling. Despite a small increase of ultimate strain for pPLA, both PLA and pPLA tensile curves were not significantly influenced by reprocessing. The increase of pPLA ductility after reprocessing was explained by an increase of the dispersion state of plasticizer inclusions as revealed by atomic force microscope observations.

At the molecular level, size exclusion chromatography showed that PLA and pPLA suffered chain scission. This degradation mechanism was more important for PLA than for pPLA. In the case of PLA, reprocessing produced shorter chains that may act as plasticizers increasing chain mobility. Such changes were revealed in the non-isothermal testing in which a cold crystallization appeared for PLA after 3 processing cycles. Moreover, the spherulitic growth rate as well as the overall crystallization rate were increased as the number of processing cycles increased. In contrast, the pPLA had a chain mobility already improved (i.e., due to the enhanced plasticization effect), which is maintained regardless of the number of processing cycles employed. It results that crystallization kinetics of pPLA was not influenced by reprocessing.

To better fit with real conditions in use, the simulation of PLA and pPLA recycling should include a step of accelerated thermal and photochemical ageing. Therefore, the influence of ageing on the crystallization kinetics of recycled PLA and pPLA could be investigated in a further work.

#### Acknowledgments

Fonds National de la Recherche (FNR) Luxembourg is acknowledged for the grant of these research activities through the framework CORE programme with reference C13/MS/5837188. Patrick Markus from Bruker Nano Surfaces Division is also acknowledged for the AFM imaging. The POLYMAT/UPV/EHU team would like to acknowledge funding from the following projects: “UPV/EHU Infrastructure: INF 14/38”, “Mineco/FEDER: SINF 130I001726XV1/Ref: UNPV13-4E-1726” and “Mineco MAT2014-53437-C2-P”. R.A.P-C gratefully acknowledges the award of a PhD fellowship by POLYMAT Basque Center for Macromolecular Design and Engineering.

#### Appendix A. Supplementary data

Supplementary data related to this article can be found at <http://dx.doi.org/10.1016/j.polymerdegradstab.2018.01.009>.

## References

- [1] K.J. Jem, J.F. van der Pol, S. de Vos, Microbial lactic acid, its polymer poly(lactic acid), and their industrial applications, in: G.G.-Q. Chen (Ed.), *Plastics from Bacteria: Natural Functions and Applications*, Springer Berlin Heidelberg, Berlin, Heidelberg, 2010, pp. 323–346.
- [2] S. Madival, R. Auras, S.P. Singh, R. Narayan, *J. Clean. Prod.* 17 (2009) 1183–1194.
- [3] S. Papong, P. Malakul, R. Trungkavashirakun, P. Wenunun, T. Chom-in, M. Nithitanakul, E. Sarobol, *J. Clean. Prod.* 65 (2014) 539–550.
- [4] O. Martin, L. Avérous, *Polymer* 42 (2001) 6209–6219.
- [5] N. Ljungberg, B. Wesslén, *Biomacromolecules* 6 (2005) 1789–1796.
- [6] M. Rahman, C.S. Brazel, *Prog. Polym. Sci.* 29 (2004) 1223–1248.
- [7] S. Jacobsen, H.G. Fritz, *Polym. Eng. Sci.* 39 (1999) 1303–1310.
- [8] J.M. Ferri, D. Garcia-Garcia, N. Montanes, O. Fenollar, R. Balart, *Polym. Int.* 66 (2017) 882–891.
- [9] K. Wang, B. Brüster, F. Addiego, G. Kfoury, F. Hassouna, D. Ruch, J.-M. Raquez, P. Dubois, *Polym. Int.* 64 (2015) 1544–1554.
- [10] G. Kfoury, F. Hassouna, J.-M. Raquez, V. Toniazzo, D. Ruch, P. Dubois, *Macromol. Mater. Eng.* 299 (2014) 583–595.
- [11] V. Piemonte, *J. Polym. Environ.* 19 (2011) 988–994.
- [12] G. Davis, J.H. Song, *Ind. Crop. Prod.* 23 (2006) 147–161.
- [13] I. Pillin, N. Montrelay, A. Bourmaud, Y. Grohens, *Polym. Degrad. Stabil.* 93 (2008) 321–328.
- [14] M. Żenkiewicz, J. Richert, P. Rytlewski, K. Moraczewski, M. Stepczyńska, T. Karasiewicz, *Polym. Test.* 28 (2009) 412–418.
- [15] R. Scaffaro, M. Morreale, F. Mirabella, F.P. La Mantia, *Macromol. Mater. Eng.* 296 (2011) 141–150.
- [16] J.D. Badia, L. Santonja-Blasco, A. Martínez-Felipe, A. Ribes-Greus, *Bioresour. Technol.* 114 (2012) 622–628.
- [17] A. Soroudi, I. Jakubowicz, *Eur. Polym. J.* 49 (2013) 2839–2858.
- [18] D. Rasselet, A. Ruellan, A. Guinault, G. Miquelard-Garnier, C. Sollogoub, B. Fayolle, *Eur. Polym. J.* 50 (2014) 109–116.
- [19] A.J. Müller, M. Ávila, G. Saenz, J. Salazar, Crystallization of PLA-based Materials, in: *Poly(lactic Acid) Science and Technology: Processing, Properties, Additives and Applications*, The Royal Society of Chemistry, 2015, pp. 66–98 CHAPTER 3.
- [20] B. Brüster, F. Addiego, F. Hassouna, D. Ruch, J.M. Raquez, P. Dubois, *Polym. Degrad. Stabil.* 131 (2016) 132–144.
- [21] A.T. Lorenzo, M.L. Arnal, J. Albuérne, A.J. Müller, *Polym. Test.* 26 (2007) 222–231.
- [22] S. Matsuoka, *Relaxation Phenomena in Polymers*, Hanser Gardner Publications, 1992.
- [23] R. Androsch, M.L. Di Lorenzo, C. Schick, *Eur. Polym. J.* 96 (2017) 361–369.
- [24] R. Androsch, C. Schick, M.L. Di Lorenzo, *Adv. Polym. Sci.* (2018) 235–272.
- [25] P. Pan, B. Zhu, Y. Inoue, *Macromolecules* 40 (2007) 9664–9671.
- [26] K. Aou, S.L. Hsu, L.W. Kleiner, F.-W. Tang, *J. Phys. Chem. B* 111 (2007) 12322–12327.
- [27] G. Stoclet, R. Seguela, J.M. Lefebvre, C. Rochas, *Macromolecules* 43 (2010) 7228–7237.
- [28] E.W. Fischer, H.J. Sterzel, G. Wegner, *Kolloid-Z. Z. Polym.* 251 (1973) 980–990.
- [29] Y. Tezuka, *Topological Polymer Chemistry: Progress of Cyclic Polymers in Syntheses, Properties, and Functions*, World Scientific, 2013.
- [30] L. Mandelkern, *Crystallization of Polymers: Volume 2, Kinetics and Mechanisms*, Cambridge University Press, 2004.
- [31] J.E. Mark, *Physical Properties of Polymers Handbook*, Springer New York, 2007.
- [32] J.D. Hoffman, C.M. Guttman, E.A. DiMarzio, *Faraday Discussions of the Chemical Society* vol. 68, (1979), pp. 177–197.
- [33] B. Kalb, A.J. Pennings, *Polymer* 21 (1980) 607–612.
- [34] M. Avrami, *J. Chem. Phys.* 7 (1939) 1103–1112.
- [35] M. Avrami, *J. Chem. Phys.* 8 (1940) 212–224.
- [36] M. Avrami, *J. Chem. Phys.* 9 (1941) 177–184.
- [37] A.T. Lorenzo, A.J. Müller, *J. Polym. Sci. B Polym. Phys.* 46 (2008) 1478–1487.
- [38] R. Vasanthakumari, A.J. Pennings, *Polymer* 24 (1983) 175–178.